Density control by pellets in plasmas with ELM mitigation by RMPs in the ASDEX Upgrade tokamak

M Valovič[1], P T Lang[2], A Kirk[1], W Suttrop[2], M Cavedon[2], M Dunne[2], R Fischer[2], L Garzotti[1], L Guimarais[2], N Leuthold[2], P J Mc Carthy[3], H Meyer[1], A Mlynek[2], B Ploeckl[2], E Poli[2], G Tardini[2], E Viezzer[2], E Wolfrum[2], the ASDEX Upgrade team[2] and the EUROfusion MST1 team[4]

[1]*CCFE, Culham Science Centre, Abingdon, OX14 3DB, UK*
[2]*Max-Planck-Institut für Plasmaphysik, Boltzmannstrasse 2, D-85748 Garching, Germany*
[3]*Department of Physics, University College Cork, Cork, Ireland*

[4]*See H. Meyer et al., Nucl. Fusion* ***57*** *(2017) 102014*

E-mail: martin.valovic@ukaea.uk

Abstract. This paper describes the extension of the previous experimental database on density control by pellets and ELM control by RMPs in the ASDEX Upgrade tokamak. A stationary low triangularity plasma is sustained by simultaneous pellet fuelling and RMP ELM control at ion pedestal collisionality of $\nu_{*i,ped} \sim 0.5$. Refuelling of the RMP induced density pump-out requires a pellet rate of $\Phi_{pel} \sim 0.073 P_{aux} / T_{t,ped}$. The duration of refuelling of density pump-out can be minimised to about 3 energy confinement times. Pellet fuelling increases or preserves ion pedestal pressure with respect to unfuelled ELM suppressed/mitigated phase. Pellets cause transition from ELM suppression to ELMy regime: At low triangularity, the first pellet triggers a transition to an ELMy phase but subsequent ELMs are not modulated by pellets. At elevated triangularity, initial pellets trigger ELM-like events but in-between pellets ELM suppression is preserved. In later phase, as density increases the plasma transitions to an ELMy phase similar to low triangularity case.

1. Introduction

In tokamak fusion reactors like ITER, the plasma density should be carefully controlled during all phases of the plasma evolution. Plasma density should fulfil multiple requirements imposed by such factors as avoidance of beam shine through, optimisation of transition to high confinement mode (H-mode), mitigation of edge localised modes (ELMs), maintaining at least a partially detached divertor, and maintaining the required fusion power [1]. During the main burn phase the plasma will be in H-mode when density control by neutral gas is likely to be inadequate due to an opaque scrape-off-layer [2] and fuelling by frozen deuterium and tritium pellets will be the main density control tool in ITER [3].

H-mode is usually accompanied by ELMs which are not compatible with long term divertor operation and therefore ELM control has to be applied. One of the ELM control techniques is the application of external Resonant Magnetic Perturbations (RMPs) [4, 5, 6, 7] and such a system is planned on ITER [8].

Both aforementioned actuators, pellet fuelling and RMPs, affect the outer part of the plasma and therefore it is not surprising that the density and ELM control loops are not independent. On one hand, pellets can affect the ELMs by direct ELM triggering or by modulation of the ELM frequency. On the other hand, ELM control by RMPs can affect the plasma density, in particular density reduction

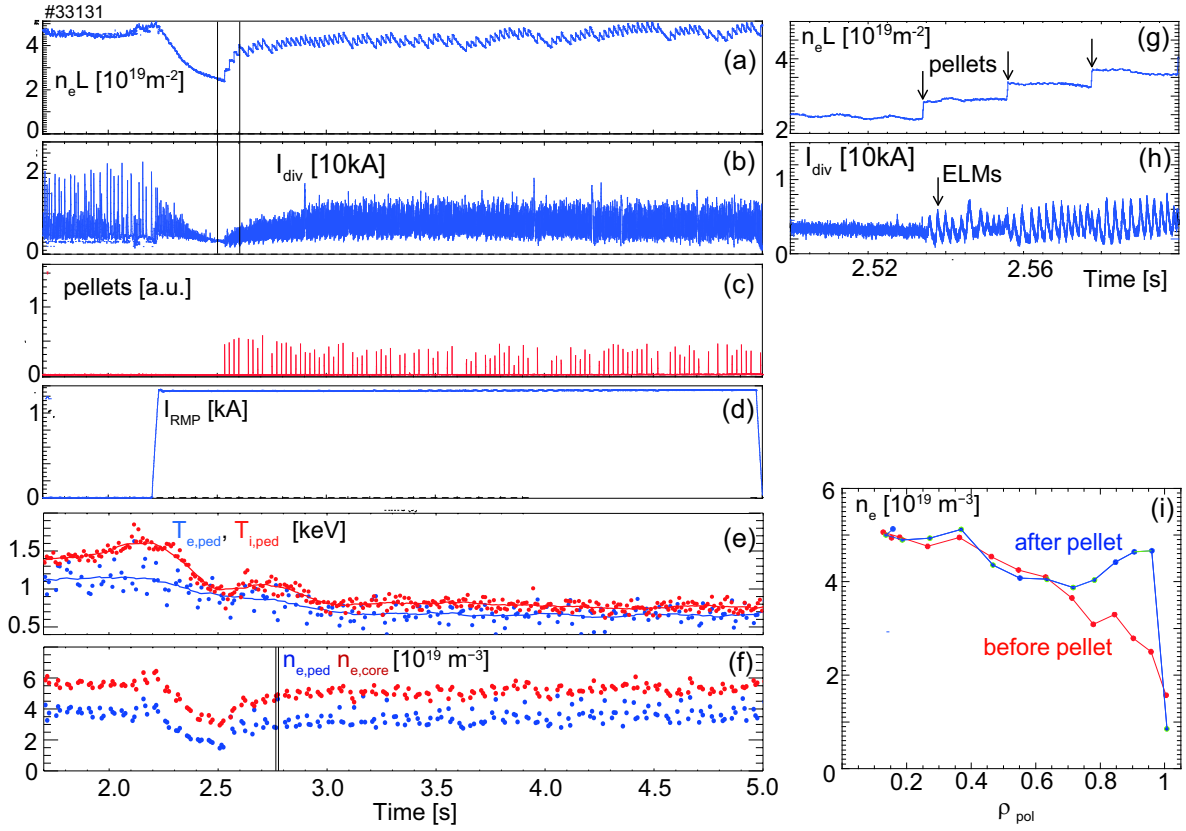

Figure 1. Temporal evolution of plasma parameters with ELM mitigation and pellet fuelling. (a) Line integrated density on the central chord, (b) outer divertor tile current, (c) pellet ablation radiation monitor, (d) RMP current, (e) electron and ion pedestal temperatures at $\rho_{pol} = \sqrt{\psi_N} \approx 0.92$, where ψ_N is the normalised poloidal magnetic flux (solid lines are the time-averaged values), (f) pedestal density at $\rho_{pol} \approx 0.92$ and core density at $\rho_{pol} \approx 0.15$. (g) and (h) temporal details of line integrated density and divertor strike point current during the time interval shown by vertical lines in panels (a) and (b). (i) density profiles just before and after the pellet at the interval shown by vertical lines in panel (f).

– density pump-out. This interlink motivated a number of experiments with simultaneous density control by pellets and ELM control by RMPs such as on DIII-D [9, 4, 10, 11], ASDEX Upgrade [12, 13, 14] and MAST [15, 16]. Despite significant progress simultaneous density control by pellets and ELM control by RMPs has not yet been fully demonstrated.

This paper describes an experiment which is a continuation of previous work reported in [14]. The main improvement is a shortening of the transient phase for pellet refuelling of the RMP density pump-out and the achievement of a steady state plasma with ELM mitigation and pellets. Finally, the paper reports on pellet fuelling of plasmas where stationary ELM suppression was obtained by RMPs with elevated plasma triangularity.

2. Experimental setup

The experiment was performed on ASDEX Upgrade. This paper reports on experiments using two plasma shapes: low upper triangularity $\delta_{up} = 0.1$ and elevated triangularity $\delta_{up} = 0.28$. For low triangularity the set up is close to those used in our previous experiment [14]. The plasma has a single null divertor, with radius of the geometric axis $R_{geo} = 1.61\,\mathrm{m}$, horizontal minor radius $a = 0.495\,\mathrm{m}$,

plasma current $I_p = 0.80\,\mathrm{MA}$, toroidal field $B_T(R = 1.65\,\mathrm{m}) = 1.81\,\mathrm{T}$, safety factor $q_{95} = 3.9$. Fresh boronisation is applied to obtain low density and consequently low plasma collisionality. To improve the reliability of the discharge small gas fuelling is used with constant rate of $\Phi_{gas} = 0.27\times10^{21}\,\mathrm{at/s}$. The plasma is heated by neutral beams ($P_{NBI} = 6\ MW$) and by on axis third harmonic electron cyclotron heating ($P_{EC} = 2.6\ MW$, $f_{EC} = 140\ GHz$). Under condition of pellet fuelling the absorption of neutral beams is ~80%. The absorption of the EC power is nearly complete (>96%) but about 20% is absorbed at the edge at second harmonic resonance as calculated by TORBEAM code [17, 18]. For the elevated triangularity plasma parameters are similar: $I_p = 0.90\,\mathrm{MA}$, $B_T = 1.82\,\mathrm{T}$, $q_{95} = 3.6$, $P_{NBI} = 6\ MW$, $P_{EC} = 1.6\ MW$ and $\Phi_{gas} = 0.9\times10^{21}\,\mathrm{at/s}$. For more details on the setup at elevated triangularity see the reference [19].

Deuterium pellets are injected vertically from high field side with a velocity of 560m/s and a nominal size of $1.4\times1.4\times1.5\mathrm{mm}$. For this parameter set, a total loss by arrival in the plasma of 30% takes place reducing the effective pellet particle content to $N_{pel} = 1.2\times10^{20}\,\mathrm{atoms}$ [20] (about ~20% of plasma inventory). ELMs are controlled by RMP coils with $n = 2$ toroidal periodicity (for details see [19]).

3. Stationary plasma with pellets and RMPs at low triangularity

Figure 1 shows the traces of parameters for a discharge in which the plasma is sustained by pellet fuelling and ELMs are controlled by RMPs. At the beginning of the discharge RMPs are applied and the plasma density starts to decay. The corresponding pump-out rate determined from the slope of line integrated density is $\Phi_{RMP} = dN_e/dt|_{t=2.25s} \approx d(n_e\ell)/dt|_{t=2.25s}\, V/2a \approx 1.7\times10^{21}\,\mathrm{at/s}$. Here $(n_e\ell)$ is the horizontal line integrated density and V is the plasma volume. The rate Φ_{RMP} is $\sim 1.7\times$ larger than in our previous experiment [14]. We do not have an explanation for this stronger pump-out rate, but better boronisation and lower gas puff could be the cause (gas puff in the present experiment is $\Phi_{gas} = 0.27\times10^{21}\,\mathrm{at/s}$ compared to $\Phi_{gas} = 0.5\times10^{21}\,\mathrm{at/s}$ in our previous work [14]). Simultaneously with a density decrease the ELMs change from pre RMP mix of large and small ELMs with frequency of $f_{ELM}(2.0-2.2s) \approx 100Hz$ to fully ELM suppressed regime at t ~ 2.52s (see figure 1a, 1b and in detail 1g, 1h). During the pump-out phase the ion pedestal temperature decreases showing the degradation of pedestal ion confinement. The decrease is also seen in pedestal electron temperature but to a lesser extent (see figure 1e).

After a pause, pellets with a constant rate of $f_{pel} = 47Hz$ are applied and the density is recovered to a level close to that before application the RMPs. The corresponding pellet fuelling rate is $\Phi_{pel} = 5.6\times10^{21}\,\mathrm{at/s}$. This value is higher than in our previous experiment in [14] where $\Phi_{pel} = 1.9\times10^{21}\,\mathrm{at/s}$ was needed for the refuelling of the density pump-out. This is in line with the stronger pump-out rate mentioned above.

During the refuelling phase ELM suppression is lost and the plasma returns into an ELMy regime (see figure 1a, 1b, 1g and 1h). Nevertheless the ELM frequency is higher, $f_{ELM}(2.982-3.026s) \approx 450Hz$, and their amplitude is lower compared to the pre RMP phase consequently showing that the pellet refuelling preserves RMP ELM mitigation, though at a compromised level. The ratio of ELM frequencies during the pre RMP and pellet refuelling phases ($450Hz/100Hz = 4.5$) is however an exaggerated measure of ELM mitigation because of the reduction of energy confinement by the RMP which is not recovered by pellets. To account for this one can compare the normalised quantity $(f_{ELM}\tau_E)^{-1}$ which is a proxy to the relative energy loss per ELM $\delta W_{ELM}/W$ and τ_E is the thermal energy confinement time. During the pre RMP phase $(f_{ELM}\tau_E)^{-1} = (100Hz\times0.066s)^{-1} = 15\%$ while during the pellet refuelling phase $(f_{ELM}\tau_E)^{-1} = (450Hz\times0.037s)^{-1} = 6\%$ (here $\tau_E[2.15s;3.0s] = [0.066;0.037]s$). Therefore even in

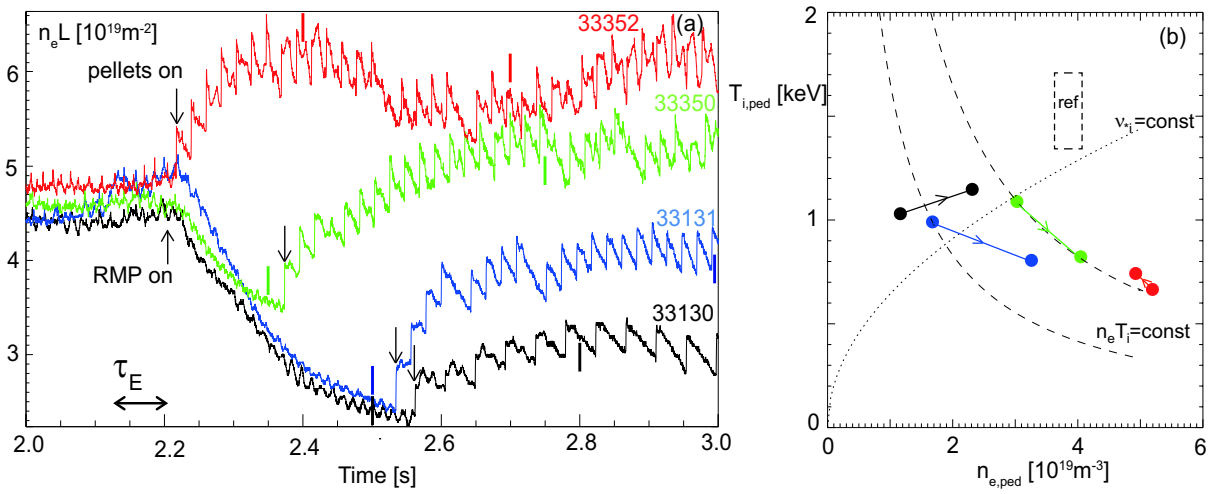

Figure 2. Refuelling of the RMP density pump-out by pellets with different timing and frequency. (a) Evolution of the line integrated density on the central chord during application of the RMP field and pellets. The timing of the RMP is the same and it is indicated by the upward arrow. The start of pellet trains is indicated by the downward arrows. The pellet rate is 23Hz for the shot 33130 and 47Hz for the shots 33131, 33350, 33352. (b) Pellet refuelling in density – temperature diagram at pedestal top $\rho_{pol} \approx 0.92$. For each shot data for two time slices are shown: start of pellet train and end of pellet transient (exception is the shot 33352 where the first point is the time of maximum density by pellets). The times selected are indicated by colour coded vertical bars on panel (a) and are as follows: #33130 (2.50s→2.80s), #33131 (2.50s→3.0s), #33350 (2.35s→2.75s), #33552 (2.40s→2.70s). The colour coding is the same as in panel (a). The box "ref" is the envelope of reference points just before RMPs including the pre-RMP pre pellet time slice for shot 33352. The dashed lines represent the contours of $n_{e,ped}T_{i,ped} = \text{const}$. The dotted line represents the contour of $\nu_{*i,ped} = 0.25$, where $\nu_{*i,ped} = 4.9 \times 10^{-18} q R_{geo} n_{i,ped}(m^{-3}) Z^4 \ln\Lambda_{ii} / (T_{i,ped}^2 \varepsilon^{3/2})$, $\ln\Lambda_{ii} = 17$, $\varepsilon = a/R_{geo}$, $Z = 1.5$, $n_{i,ped} = n_{e,ped}/Z$ [21].

normalised units pellet refuelling still preserves some of the ELM mitigation (a factor of 2.5) compared to the pre RMP phase. Note that a similar value was found in our previous paper [14].

Regarding the type of ELMs during the stationary pellet refuelling phase let us note that in our previous work [14] conventional 2D pedestal stability analysis showed that peeling-ballooning modes are stable during the pellet refuelling phase, perhaps indicating that ELMs are not type-I. Another favourable observation is that during the stationary phase individual pellets do not affect ELMs neither by triggering prompt large ELMs nor by modulation of the ELM frequency. In this context the volume averaged effective charge Z_{eff} is decreasing during pellet fuelling phase and is below ~1.5 .

The pellet fuelling phase is sustained for more than 2 seconds and it is terminated only by engineering settings. During this phase the line integrated, core and pedestal plasma densities are both stationary showing that the density profiles are also not evolving (see figure 1a and 1f). It has to be noted that the line integrated density signals in figure 1a, and elsewhere in this paper, are measured by DCN interferometer which can be affected by fringe jumps during the pellet injections. For this reason special correction procedure is used [22] and the signals are compared with the CO_2 interferometer so that there are no fringe jumps.

Figure 1f shows the pedestal density signal measured by Thomson scattering. The scatter is caused by the arbitrary timing of measurements relative to the pellet injection. Figure 1i shows the density profiles captured by Thomson scattering just before and just after the pellet. It is seen that the

pellet is deposited within $\rho_{pol} > 0.7$ of normalised minor radius which is similar to that expected in ITER. The local density perturbation due to the pellet is up to 50% which is about two times larger compared to the maximum value expected in ITER [23]. It is seen in figure 1f that during the pellet circle the density profile oscillates between hollow and conventional peaked shapes. In the core the density is approximately constant during the pellet circle and approaches the value before the application of RMPs. This is evident from the line integrated density signal in figure 1a and the core density signal in figure 1f showing that the pellet fuelling approximately restores the density pump-out. Regarding the evolution of density profiles during the whole phase of pump-out and refuelling we refer to our previous paper [14] where figure 4 shows three density profiles: before RMPs, during RMP after the pump-out and after the pellet refuelling. It is seen that the core density after pellet refuelling approximately matches its pre RMP value.

Figure 1e shows the evolution of electron and ion temperatures at the pedestal top. It is seen that after transients due to RMPs and pellets (discussed in the next section) the temperatures are stationary with the ion temperature somewhat larger than the electron one. In this context it is instructive to compare the time-averaged pellet fuelling flux with a normalised heat flux:

$$\Phi_{pel} \sim 0.073\, P_{aux} / T_{i,\mathrm{ped}} \tag{1}$$

Here, $T_{i,\mathrm{ped}} \sim T_{i,92} = 700eV$, $P_{aux} = 8.6MW$ is the applied power, $T_{i,92}$ is the ion temperature at $\rho_{pol} = \sqrt{\psi_N} \approx 0.92$, where ψ_N is the normalised poloidal magnetic flux, and all values represent time averages over multiple pellets during stationary phase. The front coefficient in equation (1) is in good agreement with the value found in our previous work [14] where $\Phi T_{i,ped} / P_{aux} \sim 0.05$ despite the fact that the pellet fuelling rate is lower and the pedestal temperature is higher. This indicates some similarity in character of particle transport in both cases.

4. Pellet refuelling transients at low triangularity

The shot in figure 1 is one of the series in which we tried to minimise the duration of density transient during refuelling. In an ideal case, the increase of particle transport due to an increase of RMP field should be instantly compensated by an increased fuelling acting in a feedback loop. Such control loop systems are under development. In the present work we restrict ourselves to a situation where both pellets and RMP current are set in feed forward mode as seen figure 2a. The scan starts with an application of a 23Hz pellet train starting at 2.55s (shot 33130). This pellet injection rate was not enough to refuel the density pump-out and for the rest of the scan we used pellet trains with a 47Hz pellet rate. Figure 2a shows three such shots in which the delays of the pellet trains were gradually reduced up to the point where the pellet train starts simultaneously with the application of a RMP current. It is seen that after a certain transient phase, the plasma density relaxes to the value which is broadly the same as before the application of the RMP current. These transient phases last approximately:

$$\Delta t_{refuel} \sim 0.2s \sim 3\tau_E \tag{2}$$

where $\tau_E \sim 0.066s$ is the thermal energy confinement time before the application of RMP taken at 2.15s. The timescale (2) should be considered as a typical response time for combined density and ELM control feedback systems in future.

The duration of density transient (2) is approximately what is expected from the typical ratio of heat and particle diffusivities. The concern about the increased duration of the core fuelling phase was raised from the observation after the transition to H-mode in JET [24]. This effect was later supported

by gyrokinetic simulations based on of MAST [25], JET [26] and ASDEX Upgrade [27] data showing that an inverted density gradient has a stabilising effect on microturbulence and thus could reduce the inwards particle flux. It has to be noted that such a stabilising effect could be counterbalanced by a destabilising effect of an increased temperature gradient caused by a nearly adiabatic pellet deposition [28]. Another counter effect is the transient nature of a hollow density profile due to an outward loss due to ELMs or inter ELM convection (see figure 1i). The detailed analysis of particle transport during a pellet cycle is important but is outside the scope of this paper.

The next interesting observation is the changing character of pellet particle confinement as inferred from post pellet density decay time (see figure 2a). At low density the decay time is long (shots 33130, 33131 at ~2.55s) as displayed by a stair-like shape of the density signal. As density increases the post pellet decay time becomes shorter and the density signal displays a sawtooth-like behaviour. The extreme case is the shot 33352 where pellets were applied simultaneously with an RMP current. Here the pellet averaged density initially increases and then relaxes. This relaxation shows that the increase of particle transport by RMPs is also present at higher densities. (The secondary density increase in the shot 33352 starting from 2.8s coincides with the loss of ECRH power and therefore it is not related to the pellet refuelling transient). Note that in some ASDEX Upgrade experiments with gas fuelling the application of RMPs can lead to a density increase [6] and this effect is linked to the formation of high field side high density (HFSHD) front of the plasma edge. This uniformity of pellets and RMPs as actuators observed in our experiment would be a welcoming simplification for the design of feedback loops for ITER: pellets always increase the pedestal density while RMPs always decrease the density. Note however that HFSHD front could be also present on ITER despite the low collisionality and therefore extrapolation of the aforementioned observation should be further investigated.

The last observation is related to the effect of pellet refuelling on pedestal confinement. As shown in figure 1 the application of RMPs reduces plasma temperature and the subsequent pellet train introduces another temperature change. In all cases the response is stronger on ions compared to electrons. Figure 2b summarises the pedestal behaviour during the pellet refuelling phase. It is seen that in cases in which the plasma density was allowed to drop significantly the application of pellets increases ion pressure (shots 33130, 33131). In cases where the target plasma density was higher the response of ions to pellet refuelling is isobaric (shots 33350, 33352). One possible parameter which could separate these two cases is the collisionality as indicated in figure 2b. This might be quite suggestive as collisionality is also proposed as one of the possible parameters to control RMP ELM mitigation [29]. Clearly a larger dataset is needed to make a firm conclusion. Here we note that for shot 33131 the ion pedestal collisionality changes from $\nu_{*i,ped}=0.18$ to 0.51 during the pellet refuelling (trajectory in figure 2b). For comparison in our previous work after refuelling $\nu_{*i,ped}=0.21$ [14]. For the case of shot 33352 the collisionality at $t=2.7s$ is $\nu_{*i,ped}=0.92$ showing that the cases in figure 2b cover a range of collisionalities. In shot 33352 the ELM frequency is $f_{ELM}=240Hz$ and the normalised quantity $(f_{ELM}\tau_E)^{-1}=(240Hz\times 0.050s)^{-1}=8\%$. This value of $(f_{ELM}\tau_E)^{-1}$ is larger than in the lower collisionality case of shot 33131 ($(f_{ELM}\tau_E)^{-1}$=6%) perhaps indicating the change of ELM mitigation with the change in collisionality.

5. Higher triangularity plasmas

As shown above, ELM suppression can be achieved at low upper triangularity plasma shape (see figure 1). Nevertheless, in order to access the fully stationary ELM suppression phase the upper triangularity has to be elevated to about $\delta_{up}=0.28$ [19, 30]. Here we describe the first results from ASDEX Upgrade in which pellets were injected into ELM suppression phases with elevated triangularity. Figure 3 shows

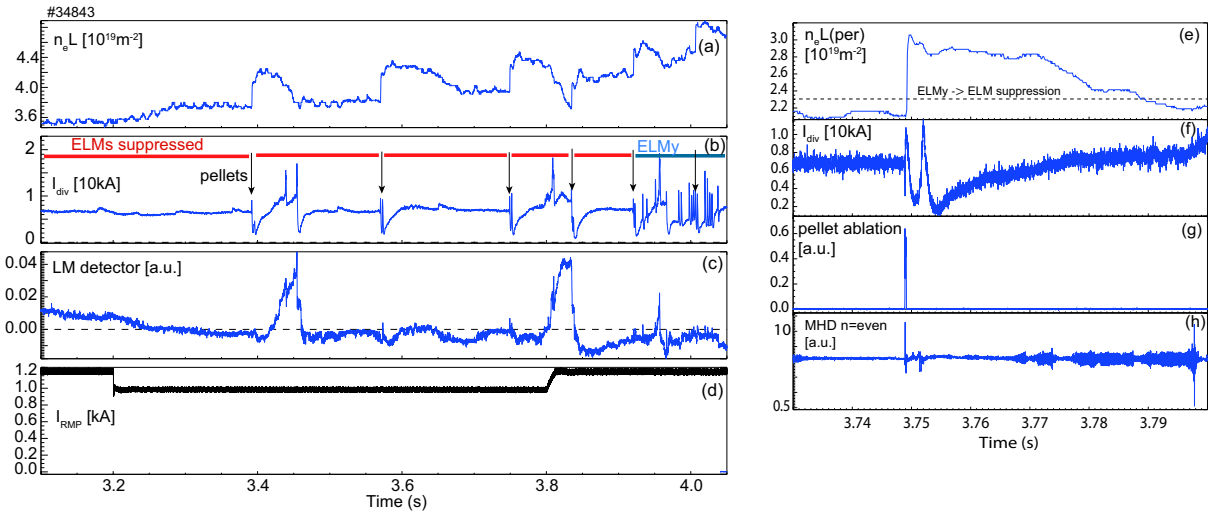

Figure 3. Panel on the left: Temporal evolution of plasma parameters with ELM suppression and pellet fuelling at elevated triangularity. (a) line integrated density on central chord, (b) divertor strike point current, ELM suppressed and ELMy phases are indicated by red and blue bars, pellets timings by arrows; (c) locked mode detector signal, (d) RMP current. Panel on the right: Expansion of the signals around 3rd pellet at 3.7s. (e) Line integrated density on peripheral chord ($\rho_{pol} > 0.8$), dashed line shows a value of the density at the transition from ELMy to ELM suppression regime earlier in the discharge. (f) divertor strike point current, (g) pellet ablation light, (h) MHD detector signal.

time traces of such a plasma. The pellet injection geometry, size and velocity are the same as in aforementioned low triangularity plasmas but the pellet frequency was deliberately lower in order to document in detail the ELM behaviour during slow density ramp. With full amplitude of RMP field each pellet triggered a transient locked mode which then dominated the post pellet density evolution. To avoid this the RMP current was reduced by 20% from 3.2s to 3.8s (see figure 3d). This has led to a reduced locked mode occurrence, as intended, but also to an increase of plasma density at 3.3s despite an unchanged gas rate. The 1st pellet still triggers a locked mode but subsequent pellets do not, as seen on the locked mode detector signal in figure 3c (interestingly second locked mode event at 3.8s seems to be removed by subsequent pellets). Overall the response of the plasma to pellets is similar to that in the low triangularity case: during the pellet train plasma density increases and at a certain point (after the pellet at 3.92s in figure 3) ELM suppression is lost and the plasma enters the ELMy regime. However, there are some differences in the details. Firstly, after transition to the ELMy phase, ELMs are more irregular compared to the almost regular ELMs in the low triangularity case (see figure 1h). The second difference is that the ELM suppression is preserved in-between initial pellets compared to the low triangularity case where already the first pellet terminates the ELM suppression, despite the pellet size being the same. This favourable observation indicates that increased triangularity makes the ELM suppression more resilient against fuelling pellets. Similarly as in low triangularity case the volume averaged effective charge Z_{eff} is decreasing during pellet fuelling phase and is below ~1.4.

Nevertheless even pellets which preserve ELM suppression trigger ELM like events as seen in the expanded view in figure 3e-h. The first event coincides with the pellet ablation and has the typical signatures of a pellet triggered ELM. About 2.5ms later there is a second event with ELM signatures on the divertor current and magnetic pick up coil signals (see figures 3f, 3h). This event is also associated with a drop in the peripheral plasma density as measured by interferometer chord at $\rho_{pol} > 0.8$ (~20% of the density increase by pellet, see figure 3e). What causes the second ELM like event is not known.

A possible explanation could be hidden in the sudden drop and slow (~200ms) recovery of the divertor tile current signal after pellets (see figures 3b, 3f). One can speculate that pellets restore the sharp density gradient just inside the separatrix to the pre RMP value and consequently destabilises ELMs (see figure 1i). The duration of this phase would be limited by the subsequent recovery of the ELM suppressed phase (see the divertor tile current in figure 3f) and thus only a limited number of ELMs are triggered. However sometimes an additional ELM occurs after a relaxation of the pedestal back to the pre pellet values and therefore cannot be explained by the transient increase of density pressure gradients due to the pellet. Another possible explanation could be that the second post pellet ELM is a result of a transient increase of q_{95} after the pellet deposition. Indeed in the case in fig 3e, q_{95} (calculated by CLISTE code [31]) gradually increases from $q_{95}(3.749s) = 3.69 \pm 0.1$, at the pellet deposition and the first ELM, to $q_{95}(3.752s) = 3.82 \pm 0.1$ when the second ELM is triggered. Including the errors bar this change might be just enough to move the plasma from ELM suppressed to ELMy regime [19]. In this context it is interesting to note that after each pellet the peripheral density exceeds the value below which the transition from ELMy to ELM suppression happened earlier in the discharge (see figure 3e). The peripheral density stays above this value much longer than the duration of the phase with two post pellet ELMs described above and therefore the simple peripheral density does not separate ELMy and ELM suppression phases. Regarding the collisionality we do not have stationary, pellet-fuelled high triangularity plasmas to evaluate values averaged over pellet cycle. Single time point measurement after the pellet in figure 3e gives $\nu_{*i,ped}(3.77s) = 0.38$, i.e. in the same range as in low triangularity case. Clearly more data is required to understand all these phenomena.

6. Conclusions

This paper reports on the significant extension of the previous experimental database [14] regarding the density control by pellets and ELM control by RMPs in the ASDEX Upgrade tokamak. New data show that:

- Stationary, low triangularity plasmas can be sustained by simultaneous pellet fuelling and RMP ELM control. The pellet rate required for refuelling of the density pump-out is $\Phi_{pel} \sim 0.073\, P_{aux} / T_{i,\mathrm{ped}}$.
- In these plasmas, the refuelling transient can be minimised to $\sim 3\tau_E$ and density control is not lost by the transient overfuelling. Pellet refuelling increases or preserves ion pedestal pressure, though below pre RMP phase.
- Pellets cause transition from the ELM suppressed to an ELMy regime. At low triangularity, this transition is sudden, but ELMs are still mitigated (compared to pre RMP phase) and their size/frequency is not modulated by the pellets. At elevated triangularity, each pellet triggers ELM-like events but ELM suppression can be preserved in-between pellets. After several pellets the plasma transitions to an ELMy regime.

Given the fact that pellet fuelling will most likely be the only actuator for core density control in ITER, it is important to assure its compatibility with ELM mitigation. Regimes with complete ELM suppression and its total independence on pellet fuelling should be the ideal goal towards which the future scenarios should be optimised. It has to be noted that in present experiments relative pellet size is somewhat larger than expected in ITER which might exaggerate some of the difficulties, therefore experiments addressing this would be useful.

Acknowledgements
This work has been carried out within the framework of the EUROfusion Consortium and has received funding from the Euratom research and training programme 2014-2018 under grant agreement No 633053 and from the RCUK Energy Programme [grant number EP/P012450/1]. To obtain further information on the data and models underlying this paper please contact PublicationsManager@ukaea.ac.uk. The views and opinions expressed herein do not necessarily reflect those of the European Commission.

References

[1] Kőchl F *et al* "Modelling of Transitions Between L- and H-Mode Including W Behaviour in ITER Scenarios") TH/P3-24, paper presented at 25th IAEA Int. Conf. on Fusion Energy St Petersburg, 2014
[2] Kukushkin A S, Polevoi A R *et al* 2011 *Journal of Nuclear Materials* **415** S497
[3] Maruyama S *et al* 2012 Proc.24th Int. Conf. on Fusion Energy (San Diego, 2012) ITR/P5-24 http://www-naweb.iaea.org/napc/physics/FEC/FEC2012/index.htm
[4] Evans T E *et al* 2008 *Nucl. Fusion* **48** 024002
[5] Kirk A *et al* 2012 *Phys. Rev. Lett.* **108** 255003
[6] Suttrop W *et al* 2011 *Phys. Rev. Lett.* **106** 225004
[7] Liang Y *et al* 2010 *Plasma Fusion Res.* **5** S2018
[8] Loarte A *et al* 2014 *Nucl. Fusion* **54** 033007
[9] Baylor L R *et al* 2008 Proc. 35th EPS Conf. on Plasma Physics (Hersonissos, Greece 2008) vol 32D (ECA) P 4.098
[10] Evans T E 2008 Implications of topological complexity and Hamiltonian chaos in the edge magnetic field of toroidal fusion plasmas. Chaos, Complexity And Transport: Theory and Applications. Edited by Chavanis Piere-Henri -. Published by World Scientific Publishing Co. Pte. Ltd., pp. 147-176
[11] Evans T E *et al* 2013 *Journal of Nucl. Materials* **438** S11
[12] Lang P T *et al* 2012 *Nucl. Fusion* **52** 023017
[13] Suttrop W *et al* 2011 *Plasma Phys. Control. Fusion* **53** 124014
[14] Valovič M *et al* 2016 *Nucl. Fusion* **56** 066009
[15] Valovič M *et al* 2013 *Plasma Phys. Control. Fusion* **55** 025009
[16] Valovič M *et al* 2015 *Nucl. Fusion* **55** 013011
[17] Poli E *et al* 2001 *Computer Physics Communications* **136** 90
[18] Poli E *et al* 2018 *Computer Physics Communications* **225** 36
[19] Suttrop W *et al* 2017 *Plasma Phys. Control. Fusion* **59** 014049
[20] Lang P T *et al* 2003 *Rev. Sci. Instr.* **74** 3974
[21] Sauter O, Angioni C and Lin-Liu Y.R. 1999 *Phys. Plasmas* **6** 2834
[22] Mlynek A *et al* 2010 *Review of Scientific Instruments* **81** 033507
[23] Polevoi A S *et al* 2017 *Nucl. Fusion* **57** 022014
[24] Loarte A *et al* 2013 *Nucl. Fusion* **53** 083031
[25] Garzotti L *et al* 2014 *Plasma Phys. Control. Fusion* **56** 035004.
[26] Baiocchi B *et al* 2015 *Nucl. Fusion* **55** 123001.
[27] Angioni C *et al* 2017 *Nucl. Fusion* **57** 116053
[28] Valovič M *et al* 2008 *Nucl. Fusion* **48** 075006
[29] Leuthold N *et al* 2017 *Plasma Phys. Control. Fusion* **59** 055004
[30] Evans T E *et al* 2004 *Phys. Rev. Lett.* **92** 235003
[31] Mc Carthy P J *et al* 2012 *Plasma Phys. Control. Fusion* **54** 015010